ADVANCED MATERIALS INTERFACES
www.advmatinterfaces.de

Hydrophobin-Coated Solid Fluorinated Nanoparticles for ^{19}F-MRI

Nazeeha Ayaz, Valentina Dichiarante, Claudia Pigliacelli, Jacopo Repossi, Lara Gazzera, Marta Boreggio, Daniele Maiolo, Cristina Chirizzi, Greta Bergamaschi, Linda Chaabane, Elisa Fasoli, Pierangelo Metrangolo, and Francesca Baldelli Bombelli**

In recent years, fluorine-magnetic resonance imaging (^{19}F-MRI) has emerged as a promising diagnostic technique, complementary to traditional proton magnetic resonance imaging (^{1}H-MRI) and easily translatable for clinical use, providing in-depth in vivo quantification without the use of radioactive agents. This creates a need for the development of appropriate delivery systems for highly omniphobic fluorinated probes. The use of the film-forming protein hydrophobin (HFBII) represents a sustainable and simple method to invert the philicity of fluorinated surfaces. Here, the ability of HFBII to form a rigid protein monolayer on superfluorinated coatings rendering them hydrophilic is shown, a property that is also retained in biological environment. This approach is then translated to directly disperse a solid superfluorinated ^{19}F-MRI probe, PERFECTA, in aqueous solution through the formation of core-shell hydrophobin stabilized PERFECTA nanoparticles (NPs). The obtained NPs are fully characterized in terms of morphology, magnetic properties, colloidal stability, protein corona formation, cellular viability, and imaging performance.

1. Introduction

In vivo real-time tracking of cells, molecules, and drugs in a non-invasive and quantitative way is a priority need of contemporary medicine for elucidating cell functions, monitoring pathological processes, and developing effective therapeutic strategies.[1] Among available diagnostic techniques, proton-based Magnetic Resonance Imaging (^{1}H-MRI) performs well in imaging soft tissues with no depth limitation, providing high-resolution, anatomical and functional pieces of information, without using ionizing radiation and radioactive nuclides.[2] To further enhance MRI contrast, gadolinium or iron oxide based probes are commonly used for diagnosis, however their sensitivity and specificity are limited and their safety is still debated, as devastating late adverse reaction are frequently reported or are still to be investigated.[3] As alternatives to these contrast agents, those based on fluorinated (^{19}F) compounds are turning promising providing "hot-spot" imaging features, owing to ^{19}F high gyromagnetic ratio and negligible in vivo background.[4] Following their administration, fluorinated probes can thus be directly detected and quantified with high selectivity, especially if they contain manifold magnetically equivalent ^{19}F atoms, as is the case of the recently reported superfluorinated molecular probe PERFECTA (**Figure 1**).[5] Despite its advantages, offered by a sharp ^{19}F singlet resonance peak and suitable relaxation properties, PERFECTA obviously lacks water solubility and, for biomedical applications, it needs to be dispersed in aqueous media by means of lipid emulsifiers, or by encapsulation into polymeric nanoparticles or micelles.[5,6]

In the present work, we designed a different strategy to directly disperse solid PERFECTA nanoparticles into physiological solutions by using a surfactant and film-forming protein, which self-assembled at the PERFECTA-water interface, resulting in the formation of monodisperse PERFECTA solid nanoparticles (NPs) coated by a biocompatible protein shell. To the best of our knowledge, there are only a couples of literature examples where fluorine-tagged peptides and proteins have been reported as potential water-dispersible ^{19}F-MRI probes.[7] Differently from these tagging-based approaches, we decided to rely on the noteworthy coating properties of class II hydrophobins, HFBI and

N. Ayaz, V. Dichiarante, C. Pigliacelli, J. Repossi, L. Gazzera, M. Boreggio, D. Maiolo, C. Chirizzi, E. Fasoli, P. Metrangolo, F. Baldelli Bombelli
Department of Chemistry
Materials and Chemical Engineering "Giulio Natta"
Politecnico di Milano
Milano 20131, Italy
E-mail: pierangelo.metrangolo@polimi.it; francesca.baldelli@polimi.it

G. Bergamaschi
Istituto di Scienze e Tecnologie Chimiche "Giulio Natta"
National Research Council of Italy (SCITEC-CNR)
Milan 20131, Italy

L. Chaabane
Institute of Experimental Neurology (INSpe) and Experimental Imaging Center (CIS)
IRCCS San Raffaele Scientific Institute
Milano 20132, Italy

C. Pigliacelli
Hyber Center of Excellence
Department of Applied Physics
Aalto University
Puumiehenkuja 2, Espoo FI-00076, Finland

The ORCID identification number(s) for the author(s) of this article can be found under https://doi.org/10.1002/admi.202101677.

DOI: 10.1002/admi.202101677

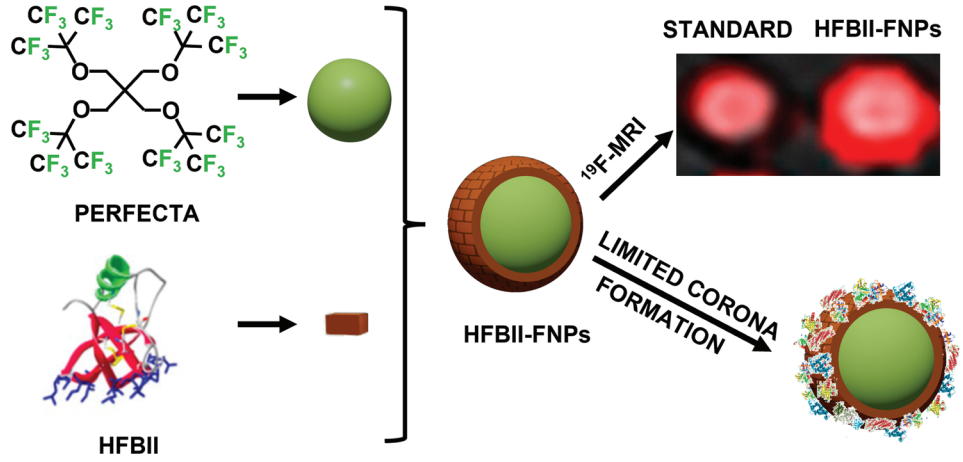

Figure 1. Cartoon showing the structure of PERFECTA NPs coated by a HFBII shell (HFBII-FNPs) and subsequent studies concerning (top) their ^{19}F-MRI properties and (bottom) their interfacial interactions with proteins in biological fluids.

HFBII, which are amphiphilic proteins produced by *Trichoderma reesei*.[8] These relatively small (≈10 kDa) globular proteins are characterized by the presence of a localized hydrophobic portion—the *hydrophobic patch*—that makes them extremely surface active, and able to self-assemble into amphipathic layers at hydrophobic-hydrophilic interfaces.[9] The fluorosurfactant abilities of HFBI and HFBII have already been successfully exploited in several applications, including the aqueous dispersion of hydrophobic and highly fluorinated materials,[10] stabilization of fluorinated oil-in-water emulsions, and fluorinated gas microbubbles for biomedical purposes,[11] as well as coating and functionalization of fluorinated surfaces.[12a] Furthermore, hydrophobins have been already shown to significantly reduce the adsorption of proteins, i.e., protein corona, on the surface of NPs, once they are exposed to biological fluids, providing efficient protection from aggregation and thus influencing their biological fate.[13]

We focused on HFBII, which is also known to form highly ordered crystalline monolayers at interfaces,[9a] but is less prone to self-aggregation in water. First, we confirmed its coating ability towards solid surfaces functionalized with a highly branched fluorinated layer, structurally similar to PERFECTA, and its tendency to reduce adsorption of serum proteins. Starting from these preliminary results on solid fluorinated surfaces, we translated this approach to the surface of fully fluorinated NPs, i.e., PERFECTA NPs. We developed a simple protocol to obtain a colloidally stable dispersion of solid PERFECTA NPs coated by a HFBII shell (HFBII-FNPs, Figure 1), at a concentration of ^{19}F atoms suitable for ^{19}F-MRI applications. These NPs were fully characterized in terms of morphology, magnetic properties, colloidal stability, protein corona, cellular viability and uptake, and imaging performance demonstrating their full potential as nanostructured probes for ^{19}F-MRI.

2. Results and Discussion

2.1. HFBII Coating Ability on Superfluorinated Surfaces

As recently reported by some of us, a highly fluorinated branched thiol, F_{27}-SH (**Figure 2**a), was able to self-assemble on gold (Au) surfaces forming a highly ordered and robust monolayer with interesting non-wetting properties towards both water and oil.[14] Since the molecular structure of F_{27}-SH closely resembles that of PERFECTA, a fluorinated thiol monolayer on planar surface was used as a model substrate. The ability of HFBII to adsorb on such a surface was evaluated measuring the static water contact angles (WCAs, **Table 1**, Figure S1, Supporting Information), before and after its exposure to a HFBII aqueous solution. As expected, the Au surface coated by a self-assembled monolayer (SAM) of F_{27}-SH was fully hydrophobic (WCA = 104°). Conversely, upon immersion of the substrate into a HFBII aqueous solution for 1 h, its wettability towards water was completely reversed becoming hydrophilic (WCA = 48°). Thus, HFBII was able to bind the fluorinated surface reversing its philicity, which actually became similar to that observed for analogous Au chips functionalized with a hydrophilic PEGylated thiol (PEG-SH, WCA = 41°).

The mass of adsorbed HFBII was determined by Quartz Crystal Microbalance with dissipation monitoring (QCM-D) experiments. Au-coated quartz crystals, functionalized with a SAM of F_{27}-SH, were treated with a 0.1 mg mL^{-1} solution of HFBII in phosphate buffer (PB, pH = 7.4) and a decrease in the measured QCM oscillation frequency was observed, indicating an increase in the adsorbed mass of HFBII. The calculated surface mass density of HFBII on the superfluorinated SAM (263 ± 25 ng cm^{-2}) was in good agreement with the value observed for a monolayer of HFBI (around 243 ng cm^{-2}).[12] Therefore, we assumed that HFBII also formed monolayers in these conditions. Furthermore, the overlapping of the frequency harmonics (n = 3, 5, 7, 9, 11) and the slight increase in dissipation indicated an essentially rigid behavior of formed HFBII film, which is likely associated with an efficient packing of the protein into a dense and crystalline monolayer (Figure S2a,b, Supporting Information).[12] Similarly, the tendency of serum proteins to bind to HFBII layer was determined treating HFBII-coated F_{27}-SH functionalized Au chips with 10% (v/v) fetal bovine serum (FBS) solution in PB at pH 7.4 (Figure S2a,b, Supporting Information). The measured frequency harmonics decrease and split upon FBS treatment, indicating adsorption of serum proteins. Interestingly, after

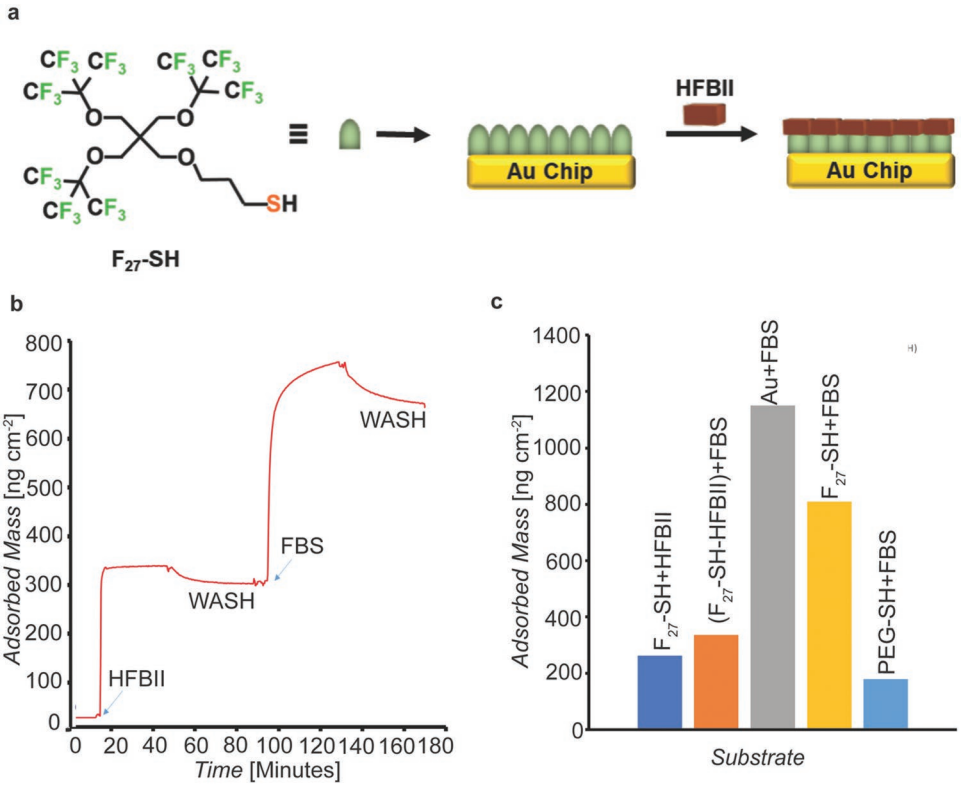

Figure 2. QCM-D measurements. a) General scheme showing the two-step functionalization of Au planar surfaces with F_{27}-SH thiol and HFBII. b) Adsorbed mass (ng cm^{-2}) on Au-quartz crystals coated with F_{27}-SH, and then flushed with HFBII and FBS solutions. c) Values of adsorbed mass (ng cm^{-2}) on QCM Au-quartz crystals after all the different functionalization treatments performed.

washing, the frequency harmonics overlap, suggesting that HFBII is not displaced, but serum proteins are simply bound on the pre-existing film. The measured surface coverage related to the adsorption of serum proteins, tightly bound to HFBII layer, resulted equal to 336 ± 11 ng cm^{-2} (Figure 2b,c). This result was compared to the adsorption of serum proteins on PEGylated substrates, as PEG is a well known, approved stealth material.[15] Experiments were performed exposing PEG-SH functionalized Au sensor surfaces to FBS solution in the same conditions (Figure 2c, Figures S2c,d and S3a, Supporting Information) and a surface mass density of 180 ± 17 ng cm^{-2} was found, in agreement with what previously reported for similar substrates.[15c,d] Moreover, control experiments on pristine and F_{27}-SH coated Au QCM crystals showed much higher protein adsorption with surface mass densities of 1150 ± 109 and 810 ± 14 ng cm^{-2}, respectively, upon FBS treatment (Figure 2c, Figures S2e–h and S3b,c).

Table 1. Static water contact angles (WCAs) measured on Au planar chips.

Substrates	WCA [°]a)
Au	20 ± 1
Au + F_{27}-SH	104 ± 6
Au + F_{27}-SH + HFBII	48 ± 3
Au + PEG-SH	41 ± 3

a)Average CA values and standard deviations based on six independent measurements.

Both HFBII and PEG coatings promoted a strong reduction in protein adsorption with respect to the pristine surfaces, but the frequency harmonics pattern of the adsorbed protein films formed on HFBII and PEG coated surfaces is clearly different: For the pegylated substrate they are more separated and do not overlap upon washing. Thus, the adsorbed films not only differ in protein concentration, but also in protein packing at the interface. Overall, these results demonstrated the ability of HFBII to form a stable film on the superfluorinated surface functionalized with PERFECTA derivative and its stability in biological environment.

2.2. Preparation and Characterization of HFBII-FNPs

On the basis of previous results, a protocol to obtain HFBII-stabilized PERFECTA NPs (HFBII-FNPs) in aqueous solution was developed (see Experimental Section for details). The obtained dispersions were first investigated by Cryogenic-Transmission Electron Microscopy (Cryo-TEM, **Figure 3**a), which revealed the presence of dark spherical NPs with a mean size of 50 ± 12 nm (Figure 3b). HFBII layer was not clearly visible due to the low contrast. Dynamic Light Scattering (DLS) multi-angle analysis of the same dispersion showed a single population with an hydrodynamic radius ⟨R_H⟩ of 88 ± 4 nm (Figure S4a, Supporting Information) and mean PDI value obtained at different angles was about 0.15 indicating a quite monodisperse NP population. Of note, a 10–20% larger size

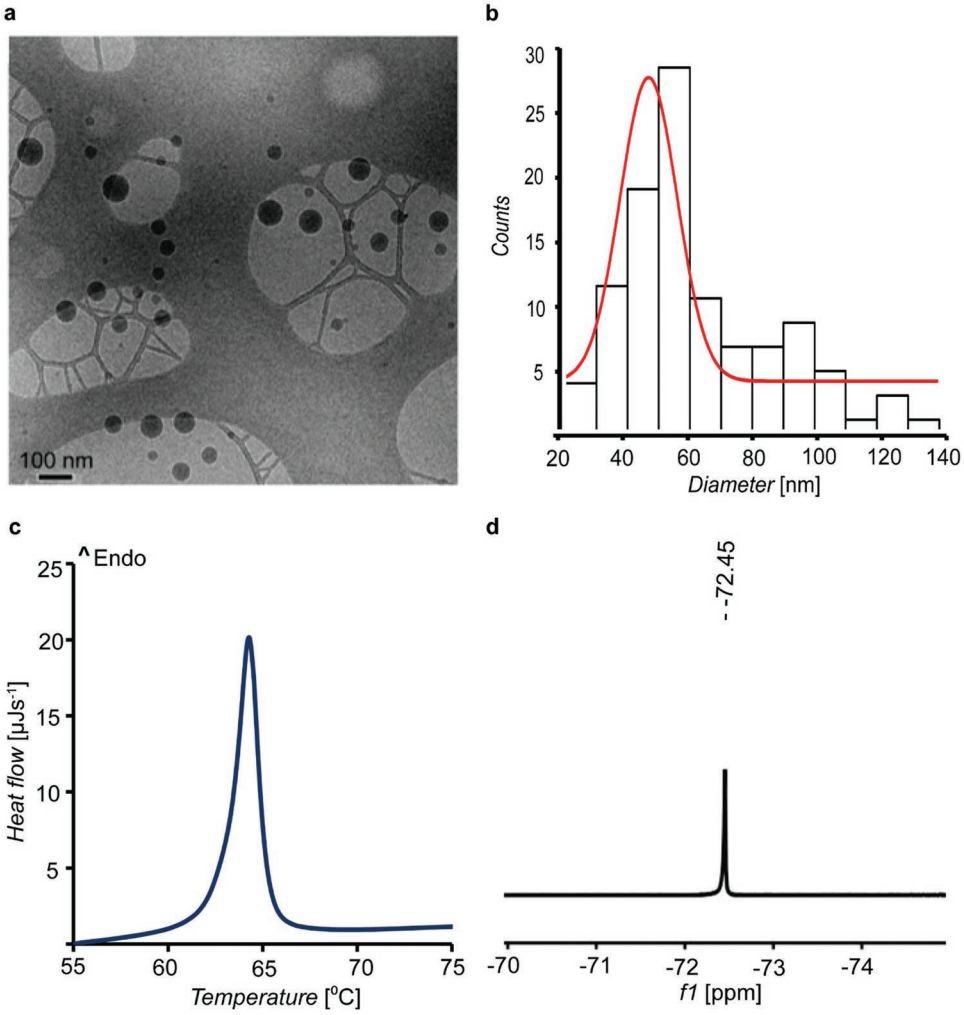

Figure 3. Characterization of HFBII-FNPs. a) Cryo-TEM image showing the presence of quite monodispersed spherical NPs. b) Statistical analysis of NP sizes imaged by Cryo-TEM. c) Micro-DSC thermogram of a PB dispersion of HFBII-FNPs. d) ^{19}F-NMR spectrum of HFBII-FNPs solution in PB (signal at –72.4 ppm).

at DLS with respect to what observed by microscopy is always expected due to protein and hydration shells included in hydrodynamic sizes. Moreover, intensity-weighted DLS size distribution are always dominated by larger size populations, while in Cryo-TEM these populations can be underestimated as sometimes larger particles are excluded during film vetrification. Colloidal stability of HFBII-FNPs was successfully monitored by DLS in PB over a period of 7 days (Figure S4b, Supporting Information). Their size was quite stable with only a slight decrease in $\langle R_H \rangle$, related to limited and reversible flocculation process. Micro-Differential Scanning Calorimetry (Micro-DSC) analysis of the same nanoformulation showed a melting transition around 64 °C, perfectly matching the melting point of solid PERFECTA (Figure 3c) and thus demonstrating that the obtained water-dispersible NPs are constituted of a solid PERFECTA core coated by hydrophobin shell. The composition of HFBII-FNPs was studied by FTIR, confirming the presence of both PERFECTA and HFBII (Figure S4c, Supporting Information).

^{19}F-NMR measurements on HFBII-FNPs dispersions showed a sharp singlet peak at –72.4 ppm (Figure 3d), and using trifluoroacetic acid (TFA) as external reference standard it was possible to quantify a fluorine concentration of $4.0 \pm 0.3 \times 10^{-3}$ M, corresponding to about $8.9 \pm 0.8 \times 10^{19}$ ^{19}F atoms per mL (Figure S5, Supporting Information), which is clearly above the detection limit of ^{19}F-MRI ($\approx 1 \times 10^{18}$ ^{19}F atoms in our settings). Longitudinal (T_1) and transverse (T_2) relaxation times were also determined by ^{19}F-NMR. Relatively short T_1 and long T_2 values are usually preferred to reduce scan time and maximize signal-to-noise ratio (SNR).[16] HFBII-FNPs showed suitable T_1 (510 ± 10 ms) and T_2 (236 ± 5 ms) values to allow their use in fast-imaging methods for ^{19}F-MRI.

Colloidal stability of HFBII-FNPs was also evaluated in acidic conditions considering that the isoelectric point (pI) of HFBII is at pH = 5.2 and thus pH variation could affect protein organization at the interface and consequently the stability of the NPs. Such an effect was, in fact, confirmed by the fact that direct preparation of HFBII-FNPs at acidic pH was

unsuccessful. Then, we simply tried to vary the pH of the preformed HFBII-FNPs dispersion from 7.4 to about 4.0 to investigate its effect on the stability of the NPs. DLS measurements showed an increase in the $\langle R_H \rangle$ and PDI upon pH variation, as reported in Table S1 (Supporting Information), also accompanied by a significantly reduced ^{19}F-NMR signal of the same dispersion (Figure S6, Table S1, Supporting Information). This behavior can be explained by a re-organization of HFBII secondary structure influencing its coating ability towards fluorinated surfaces with a reduction in the stability of the resulting NPs.[10a] Zeta-potential (Z-pot) values of HFBII-FNPs were found to vary according to pH changes from −50 mV at pH = 7.4, approaching to 0 mV at pH close to the isoelectric point of the protein, to a final positive value of +42 mV at pH = 3.7 (Table S1, Supporting Information).

2.3. Protein Corona Study

The bio-nano interactions occurring upon NPs dispersion in a biological environment play a pivotal role in their final biological properties. It is known that when NPs come in contact with biological fluids, an active biomolecular layer is formed on the NP surface.[17] The biomolecular interface organization of this layer can be divided into two components called "hard" and "soft" coronas, indicating proteins strongly bound to the NP surface (inner layer) and proteins in fast exchange with the environment (outer layer), respectively. The long-lived protein corona (HC) is considered more biologically relevant, as it persists on the NP surface for times long-enough to interact with the cellular machinery and thus represent their "biological identity."[17a,18] HCs of HFBII coated NPs made of different materials have been previously studied, showing that HC composition strongly depends on NP size and composition, while the HFBII layer was always found to remain strongly associated to the NP surface when in competition with plasma proteins.

In view of the possible application of the developed HFBII-FNPs as both cell labeling agents (in vitro)[5,19] and ^{19}F-MRI tracking agents of disease progression (in vivo),[6a,4e] their stability in biological fluids was studied. In particular, HC compositions relatively to their incubation in in vitro (10% human serum, 10HS) and in vivo (55% human plasma, 55HP) conditions were determined. As a control, the same experiments were also performed in 10% human plasma (10HP) to show the effect of protein concentration on the formation of HCs.[20] DLS experiments on HFBII-FNPs incubated in 10HS, 10HP, and 55HP conditions, in situ and isolated as HC samples (see Experimental Section for details), showed in all cases the formation of a protein corona, which determined an increase in the hydrodynamic size without causing agglomeration (Figure S7a–f, Supporting Information).

We also determined HC composition by SDS-PAGE (**Figure 4**a,b and Figure S8, Supporting Information) relative to the isolated HCs for the three measured samples together with controls (untreated HFBII-FNPs and media without NPs). Importantly, in all cases, a band at about 10 kDa could be related to HFBII (by comparison with the gel of untreated HFBII-FNPs, Figure S8, Supporting Information). The HFBII layer is retained on the NP surface when in competition to environmental proteins, in agreement with literature and QCM studies on analogous substrate treated with 10% FBS (Figure 2 and Figure S2a,b, Supporting Information). As expected, the HC formed in 10HS (HCS10) showed a less rich protein pattern, different from that of the HC formed in HP (Figure 4a). Instead, we can qualitatively observe that the protein pattern of HCs in HP at different concentrations appeared similar (Figure 4b).

Identification of HC proteins for all three samples was performed with SDS-PAGE gel electrophoresis followed by gel extraction and Mass Spectrometry (MS) analysis of the digests (ESI File 2). The identified proteins were divided in main representative classes (Figure S7g,h). Interestingly, in HS the most representative classes enriched in HC are immunoglobulins and proteins belonging to immune and inflammatory responses, i.e., opsonins, suggesting that these NPs could be primarily used to label phagocytic cells (such as macrophages, dendritic cells, etc.), for which NP cellular uptake is generally immunoglobulin-mediated and thus probably promoted by the presence of these proteins in the HC. HCs isolated from HP showed, instead, a different composition, in which the most prominent class of proteins, classified as "other," contain proteins connected to cell motility (such as actin and myosin) or to DNA packing. These proteins were not classified, as our attention was mainly focused on proteins involved in processes such as inflammation, coagulation, and immune response, which play a key role in the permanence of NPs in the bloodstream and thus affect their biodistribution (Figure 4c,d).

Interestingly, HCs from HP at different concentrations showed a relevant number of specific proteins highlighting the complexity of the HC formation process and how a simple reduction in protein concentration can significantly affect its composition, as already highlighted for different NPs.[21] Of note, an increase in protein concentration (55HP) to values relevant to *in-vivo* applications significantly reduces the amount of proteins in the HC belonging to immunoglobulins and immune response. Overall, these data showed that HFBII-FNPs are stable in physiological conditions with formation of a specific HC on the HFBII shell coating the NP surface. Clearly, more specific protein corona studies will be needed in future related to the specific biomedical application of the developed NPs.

2.4. ^{19}F-MRI Preliminary Studies

To evaluate the possible application of the developed HFBII-FNPs as imaging probes, preliminary ^{19}F-MRI experiments were performed using a 7T preclinical MRI scanner on HFBII-FNP water dispersions at different dilutions (**Figure 5**a). A good signal to noise ratio (SNR) linearity as a function of ^{19}F atom concentration was achieved. Considering an acquisition time of about 1 h, we could estimate a detection threshold (SNR > 4) of about 0.6×10^{18} ^{19}F atoms ($\approx 0.4 \times 10^{-3}$ M). These results demonstrated the suitability of these NPs as ^{19}F-MRI probe, thus additional studies on cells treated with the optimized HFBII-FNP dispersion were also performed. On the basis of preliminary protein corona studies performed in HS, we decided to use these NPs for labeling microglia like cells (BV-2: immortalized

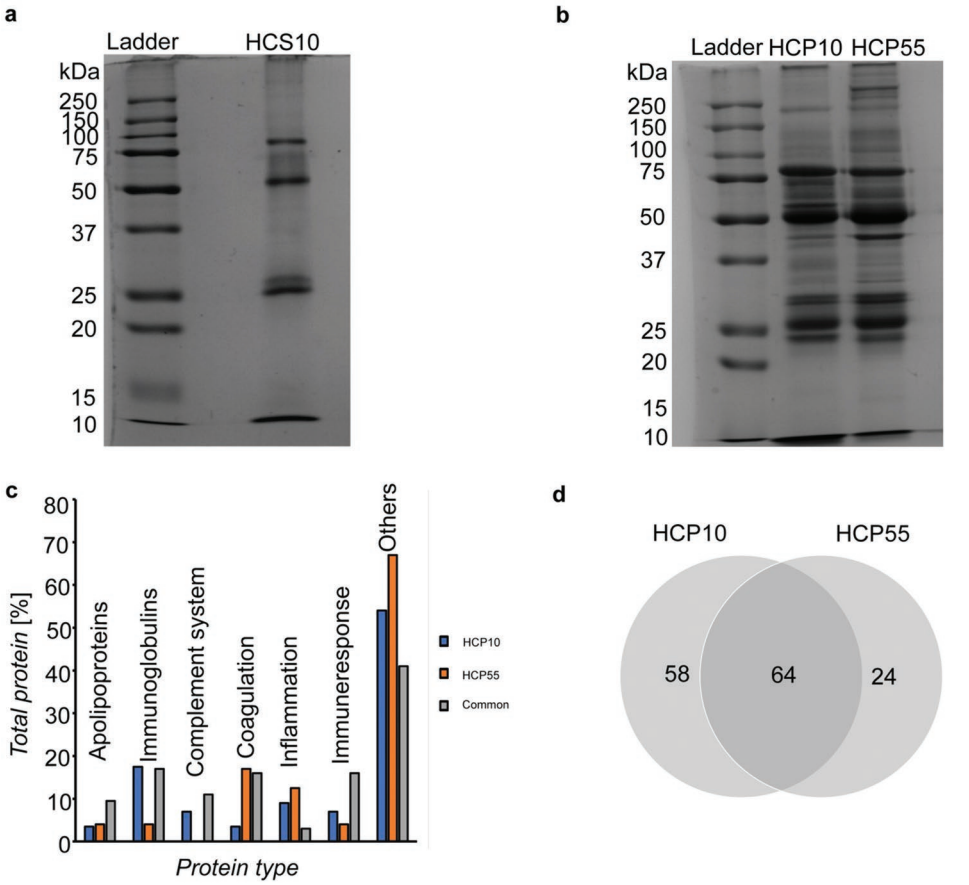

Figure 4. Analysis of Protein Corona. a) SDS-PAGE of HC isolated after incubation of HFBII-FNPs with 10% human serum (v/v). b) SDS-PAGE of HC isolated after incubation of HFBII-FNPs with10%, 55% human plasma (v/v). c) Histograms comparing specific and common proteins identified in HCP10 and HCP55. Proteins were divided in seven categories, based on biological processes they are involved in. Proteins classified as other are associated to cell motility (such as actin and myosin) or with DNA packing, like histones. d) Venn diagram to compare identified proteins in HCP10 and HCP55. Specific proteins are 48% and 27% of total proteins identified in HCP10 and HCP55, while common proteins are 52% and 73% of total proteins identified, respectively.

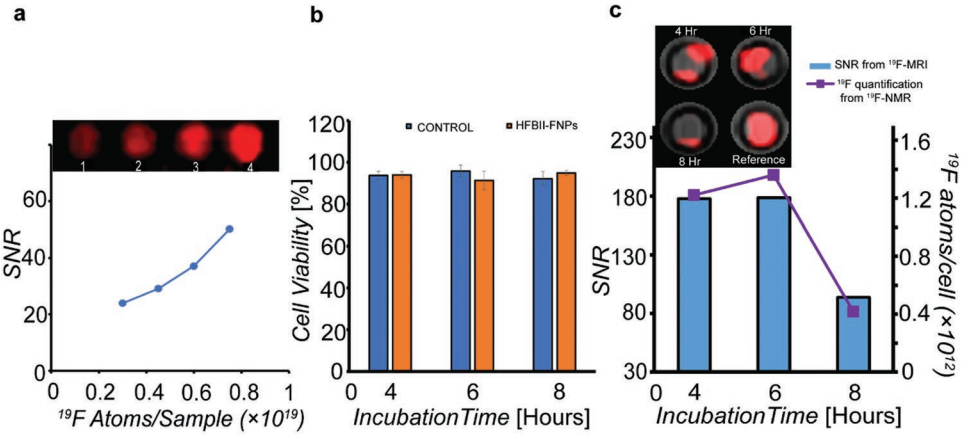

Figure 5. ^{19}F-MRI experiments on HFBII-FNP dispersions and on cells incubated with HFBII-FNPs. a) ^{19}F-MRI experiments performed on HFBII-FNPs diluted in PB at different PERFECTA concentrations [2, 3, 4, 5×10^{-3} M] indicated as 1, 2, 3, and 4, respectively, in the top image. The graph represents the relative measured SNR (signal to noise ratio) linearity with increasing ^{19}F atom concentrations. b) Cell viability assessed by trypan blue exclusion method on BV-2 cells labeled with HFBII-FNPs at 1.5×10^{-3} M concentration of ^{19}F atoms. c) ^{19}F uptake per cell quantified using both ^{19}F-NMR and ^{19}F-MRI (SNR) experiments for BV-2 cells treated with HFBII-FNPs at 1.5×10^{-3} M PERFECTA concentration for different incubation time (4, 6, 8 h). (Inset) ^{19}F-MRI of the labeled cell pellets collected after different incubation time and imaged with a standard reference of PERFECTA containing 1×10^{19} ^{19}F atoms.

murine microglial cell line), which are resident immune cells of the central nervous system with a high phagocytic activity.[22]

Cytotoxicity experiments performed on BV-2 cells after 4, 6, and 8 h of incubation with HFBII-FNPs at PERFECTA concentration of 1.5×10^{-3} M showed a viability similar to untreated cells even after 8 h of incubation (Figure 5b). The same cells were then collected and treated to be analyzed by ^{19}F-NMR and the amount of PERFECTA uptaken by cells at different time points was determined (Figure 5c). We observed that the maximum uptake was reached after 6 h of incubation (up to 1.72×10^{12} atoms per cell). This was visualized and confirmed by ^{19}F-MRI, where the fluorine content was quantified in comparison to the SNR of a standard solution of PERFECTA containing 1×10^{19} ^{19}F atoms (Figure 5c). Of note, ^{19}F uptake appeared reduced at 8 h of incubation with the NPs, but a rapid cell proliferation was also found, which explains this decrease in the resulting number of ^{19}F atoms per cell (Figure S9, Supporting Information). Overall, these results confirmed that HFBII-FNPs were taken by BV-2 cells without affecting cell vitality and maintained their excellent imaging properties upon internalization showing intense hot-spot signals in ^{19}F-MRI.

3. Conclusions

In summary, we have developed a new, simple, stable, and biocompatible water formulation of solid fluorinated nanoparticles suitable for ^{19}F-MRI. This target was achieved exploiting the formation of a self-assembled layer of a naturally occurring amphiphilic protein, hydrophobin HFBII, on the hydrophobic surface of solid NPs of the fluorinated molecular MRI probe PERFECTA. Full characterization of the resulting HFBII-FNPs in terms of morphology, magnetic properties, colloidal stability, protein corona formation, cellular viability and uptake, and imaging performance was performed. The HFBII shell demonstrated to remain adsorbed on the NP surface also when in competition with plasma proteins at physiological concentrations with the formation of a specific protein corona layer. Overall, our results definitively proved the excellent properties of HFBII-coated PERFECTA solid NPs as ^{19}F-MRI nanoprobes also in biologically relevant environment (i.e., BV-2 cells, microglia like cells) and their suitability for applications in cell labelling or *in-vivo* tracking of immune cells activity by ^{19}F-MRI.

4. Experimental Section

Materials and Methods: PERFECTA and F_{27}-SH were synthesized as reported previously.[5,23] Poly(ethylene glycol)methyl ether thiol (PEG-SH, Mn = 2000 g mol^{-1}, Figure S10, Supporting Information) and other starting materials and solvents were purchased from Sigma Aldrich and Fluorochem, and used as received. HFBII produced from recombinant strains of *T. reesei* was kindly provided by VTT Technical Research Centre of Finland. It was purified and lyophilized by RP-HPLC at CNR, Milan and stored at room temperature under vacuum. Experiments were performed using 1×10^{-3} M PB solution without chlorides (pH = 7.4). Dialysis membrane (MWCO 100 kDa) was purchased from Spectrum Laboratories.

Contact Angle Measurements: 11 × 11 mm Au(111)-coated glass chips were purchased from Arrandee metal GmbH (Germany). Prior to use, Au chips were washed with MilliQ, dried and UV-ozonized for 30 min. The chips were functionalized with thiols by dipping them in a 1×10^{-3} M ethanol solution of F_{27}-SH or 1×10^{-3} M aqueous solution of PEG-SH thiol, respectively, for 24 h, then rinsing with clean solvent and dried before measurements. Clean unfunctionalized chips were dried and used as reference. A separate set of F_{27}-SH functionalized chips were further treated with 0.1 mg mL^{-1} buffer solution of HFBII for 1 h in order to test the ability of HFBII to coat fluorinated surfaces. Static water contact angles (WCAs) were measured using the sessile drop method by placing three different drops of MilliQ (4 µL drop volume) on two different chips.

QCM-D Experiments: A Q-Sense E4 instrument quartz crystal microbalance with dissipation monitoring (QCM-D) was used to measure the adsorbed mass of HFBII and FBS on thiol-functionalized Au QCM crystals. Untreated crystals were first UV-ozonized for 10 min, then immersed at 75 °C in a $H_2O/NH_3/H_2O_2$ (5:1:1 v/v) mixture for 10 min, then rinsed thoroughly, dried and again treated in UV/ozone chamber for 10 min. The sensors were functionalized by immersing them in 1×10^{-3} M ethanolic solution of F_{27}-SH overnight at room temperature. The sensors were washed with ethanol, dried and mounted into the measurement chamber, which was maintained at 37 °C. Once the calibration and stable baseline had been established, 500 µL of 0.1 mg mL^{-1} of HFBII in PB was pumped through the measurement chambers using a flow of 100 µL min^{-1}. The sensors were then incubated for 30 min in zero-flow conditions, after which the surface was washed with running buffer for 40 min to remove the excess protein. Subsequently, 500 µL of FBS (Biowest), dissolved into the same buffer solution to a final concentration of 10% (v/v), was flowed through the chambers at the same rate. The sensors were incubated for another 30 min in zero-flow conditions and then rinsed for 40 min with buffer. PEG-SH functionalization on the QCM crystals was made by pumping 500 µL of 1×10^{-3} M aqueous solution of PEG-SH through the chamber at a flow of 100 µL min^{-1} for 5 min, followed by incubation in zero-flow conditions for 24 h. The binding of FBS on PEG-SH was tested under the same conditions as before. Control experiments were performed by exposing the sensor surfaces, both pristine and F_{27}-SH coated, to FBS solutions under the same conditions. Dissipation values larger than zero imply that the adsorbed mass will not couple 100% to the oscillatory motion of the sensor. For this reason, the true adsorbed mass would be underestimated by the Sauerbrey equation; consequently, the adsorbed masses of HFBII and FBS were here estimated using the QTools software from the frequency and dissipation changes, applying the Voigt viscoelastic model to overtones 3, 5, 7, 9, and 11.

Synthesis of HFBII-FNPs: HFBII-FNPs were synthesized by melting 10 mg of PERFECTA at 80 °C. HFBII was dissolved in 1×10^{-3} M PB (pH = 7.4) at a concentration of 0.1 mg mL^{-1}, and 1 mL of protein solution was added to melted PERFECTA and heated for 30 min at 80 °C. The sample was then sonicated using a SONIC Vibra-Cell tip sonicator (Newtown, CT) operating at 130 W and 20 kHz (70% amplitude) for 10 s. Three heating-sonication cycles were carried out, then the sample was left to rest overnight at room temperature. Unbound HFBII molecules were removed by dialysis against PB for 8 h, using a 100 kDa MWCO membrane.

Cryogenic Transmission Electron Microscopy: Cryo-TEM images were collected using JEM 3200FSC field emission microscope (JEOL) operating at 300 kV in bright field mode with Omega-type Zero-loss energy filter. Images were acquired with GATAN DIGITAL MICROGRAPH software while the specimen temperature was maintained at −187 °C. Cryo-TEM samples were prepared by placing 3 mL of sample aqueous dispersion on a 200 mesh copper grid with holey carbon support film (Holey Carbon-Cu, 200 mesh, 50 µm) and plunge freezed using vitrobot with 2 s blotting time under 100% humidity.

DLS Multiangle Analysis: Dynamic Light Scattering measurements were performed on an ALV apparatus equipped with ALV-5000/EPP Correlator, special optical fiber detector and ALV/CGS-3 Compact goniometer. The light source was He-Ne laser (λ = 633 nm), 22 mW output power. Measurements were performed at 25 °C. ≈1 mL of sample solution was transferred into a cylindrical Hellma scattering cell. Data

analysis was performed according to standard procedures and auto-correlation functions were analyzed through a constrained regularization method (Laplace inversion of the time auto-correlation functions), CONTIN, for obtaining the particle size distribution. Stability of HFBII-FNPs in biological fluids was assessed diluting the emulsion 1:2 (v/v) in Dulbecco's modified Eagle's medium (DMEM, Gibco) and solutions of FBS at 10% in DMEM, and incubating the samples at 4 °C. Plotting Z-averaged hydrodynamic diameters and PDIs versus time in days it was possible to observe that the emulsions were stable up to 1 week.

Micro-Differential Scanning Calorimetry (Micro DSC): Micro-DSC measurements were performed using a Nano-DSC from TA instruments (New Castle, DE, USA). 300 µL of HFBII-FNPs were placed in the calorimetric cell and the same volume of PB buffer solution was placed in the reference cell. A total pressure of 3 atm was applied to both cells during the temperature scanning. The heating and cooling scan were recorded at 1 °C min^{-1} in the temperature range of 20–80 °C. A reheating scan was recorded to assess the transition reversibility. Buffer-buffer scan was recorded under identical conditions in an independent experiment and subtracted from the sample scan. The excess molar heat capacity function ($\langle \Delta Cp \rangle$) was obtained after a baseline subtraction. The data were analyzed using the NanoAnalyze software package supplied with the instrument.

^{19}F-NMR Measurements: ^{19}F-NMR spectra were obtained on a Bruker AV400 spectrometer operating at 400 MHz for ^{19}F nuclei. An external capillary containing a 5.5×10^{-6} M solution of TFA in D_2O was used as the reference standard to make quantitative measurements. ^{19}F T_1 and T_2 measurements were performed at 305 K on the same spectrometer. The longitudinal relaxation times (T1) were measured using an inversion recovery (IR) sequence. The transverse relaxation times (T2) were measured using a Carr-Purcell-Meiboom-Gill (CPMG) sequence. Other parameters consisted of time delay =16(T1), 24(T2), temperature = 305 K, NS (number of scans) = 100 (T1), 64 (T2) and receive gain = 203.

Zeta-Potential: Zeta Potential (ZP) experiments were carried out using a Zetasizer Nano ZS (Malvern Instrument, Malvern, Worcestershire, UK), equipped with a 633 nm red laser and measuring the scattered light at an angle of 173°. The analysis was performed at 25 °C in folded capillary cells suitable for the measurement of zeta potential, i.e., U-shaped cells with two Au plated beryllium/copper electrodes at the top. Before each measurement, the cells were firstly cleaned with MilliQ and conditioned with the sample dispersant. Then, ≈0.8 mL of sample solution was inserted, checking that the Au-plated electrodes were immersed and that there were no bubbles inside the cell.

Protein Corona: Human plasma and human serum was purchased from Sigma Aldrich. HFBII-FNPs in PB were incubated with 10%, 55% v/v human plasma for 1 h at 37 °C and such samples were called in situ HP10 and in situ HP55. Hard corona complexes were isolated from in situ samples by sucrose cushion methodology (one centrifugation with 0.7 M sucrose cushion at 15 500 rcf at 4 °C, followed by 3 washes in PB and re-suspensions in 60 µL PB pH 7.4) and are labeled as HCP10 and HCP55.[24] In situ HS10 and hard corona (HCS10) samples were obtained by performing similar experiments with 10% human serum. Control samples (without NPs) of 10% and 55% human plasma in PB or 10% human serum in PB were treated in the same way (10HP and 55HP or 10HS). The size of pristine HFBII-FNPs was compared with in situ and HCP10, HCP55 samples by DLS measurements at 90°.

SDS-PAGE Electrophoresis: All reagents required for SDS-PAGE electrophoresis were purchased from Bio-Rad, Sigma Aldrich. 30 µL of SDS-PAGE loading buffer (Bio-Rad, 65.8×10^{-3} M Tris–HCl, pH 6.8, 2.1% SDS, 26.3% (w/v) glycerol, 0.01% bromophenol blue), supplemented with β-mercaptoethanol (1:20) were added to 60 µL of each sample (HCP10, HCP55, HCS10, 10HP, 55HP, 10HS) and kept at 99 °C for 5 min for digestion. Prior to denaturation, protein estimation of the all samples were done by BCA protein assay (Thermo Fisher Scientific). Digested hard corona samples (HCP10, HCP55, HCS10), HFBII-FNPs, as well as the control (10HS) having the same protein concentration and 5 µL of a molecular ladder (Bio-Rad) were loaded in the wells of SDS-PAGE gels. The gel was composed by a 4% polyacrylamide stacking gel (125×10^{-3} M Tris–HCl, pH 6.8, 0.1%, m/v, SDS) and a 12% resolving polyacrylamide gel (in 375×10^{-3} M Tris–HCl, pH 8.8, 0.1%, m/v, SDS buffer). A Tris-glycine buffer at pH 8.3 (with 0.1% SDS, m/v) was employed to fill the cathode, whereas a Tris buffer at pH 8.8 was used in the anode. Electrophoresis was performed with three steps with increasing voltage: first step was set at 50 V for 20 min, second step at 100 V for 40 min and third step at 150 V until the dye front reached the bottom of the gel. Staining and distaining were performed with Colloidal Coomassie Blue (Serva) and 7% (v/v) acetic acid in water, respectively. Finally, the SDS-PAGE gels were scanned with a VersaDoc imaging system (Bio-Rad).

Mass Spectrometry and Data Analysis: The lanes of SDS-PAGE were cut and treated following the standardized MS protocols, using 0.02 µg μL^{-1} trypsin (Sigma Aldrich) as digestive enzyme.[25] 8 µL of tryptic-digested samples were injected in nano-chromatography system (UltiMate 3000 RSLCnano System, Thermo Scientific), coupled with mass spectrometer (LTQ XL, Thermo Scientific).[25] The MS data were analyzed by the Mascot search engine (Version 2.3.01), using the Proteome Discoverer software (v. 1.2.0 Thermo) and consulting specific UniProtKB/Swiss-Prot protein database (taxonomy Homo sapiens 188 582 sequences and 344 584 622 residues) (Supplementary file 2). Oxidation of methionine residues was set as variable modifications; one missed cleavages were allowed to trypsin; peptide mass tolerance was set to 1 Da, fragment mass tolerance to 0.8 Da, ion source cut-off of 20 and significance threshold of $p < 0.01$.

Magnetic Resonance Imaging: All experiments were performed with a 7-T imager (Biospec; Bruker Biospin, Germany) using a dual transmit-receive ^{19}F/^{1}H volume coil. ^{19}F MR images were acquired at the specific resonance frequency of PERFECTA (-72 ppm). A three-dimensional turbo spin-echo sequence was used for ^{19}F-MRI with field of view $50 \times 30 \times 24$ mm and other parameters such as TR/TE 3000/56 ms, matrix $64 \times 32 \times 8$ and 100 signal averages. The signal-to-noise ratio (SNR) was quantified on ^{19}F images normalized to the standard deviation of noise in the background. The ^{19}F-MRI was used to visualize the HFBII-FNPs samples at different concentrations (2, 3, 4, 5×10^{-3} M) and the labeled cells.

Cellular Toxicity Experiments: BV-2 cells were cultured in DMEM (Lonza), containing 10% FBS, 100 mg mL^{-1} streptomycin, 100 U mL^{-1} penicillin and 2×10^{-3} M glutamine (Gibco-Invitrogen). Cells were split two days before seeding and used within eight passages. BV-2 cells were seeded on 6-multiwell plates (0.5×10^6 cells per well) and incubated with 1.5×10^{-3} M PERFECTA concentration of HFBII-FNPs for different timings (4, 6, 8 h). Cell viability was assessed by the standard Trypan blue exclusion method. 0.4% Trypan blue solution (Sigma Aldrich) was added to an aliquot of cell suspension (1:3 ratio). The hemacytometer was then loaded and examined immediately under a microscope at low magnification. The percentage of dead cells was estimated counting the number of blue staining cells in comparison to the total number of cells. As control, cells without HFBII-FNPs followed the same procedure using the same amount of fresh culture medium. The protocol for cell labelling and isolating the cell pellets were adapted from an optimized protocol.[6a,26] The cellular uptake of ^{19}F from the HFBII-FNP were evaluated performing ^{19}F-NMR measurements on the suspension of cellular pellets obtained after incubating the cells for different time points (4, 6, 8 h). The uptake at different time points was also checked by ^{19}F-MRI.

Supporting Information

Supporting Information is available from the Wiley Online Library or from the author.

Acknowledgements

N.A., V.D., P.M., and F.B.B. are thankful to the NEWMED project, ID: 1175999 (funded by Regione Lombardia POR FESR 2014 2020). F.B.B. and P.M. are also thankful to the project NiFTy funded by MIUR (PRIN2017, no. 2017MYBTXC). C.C. and F.B.B. are also thankful to the

P2RY12 project, ID: GR-2016-02361325 (funded by the Italian Ministry of Health). The authors acknowledge the provision of facilities and technical support by Aalto University at OtaNano—Nanomicroscopy Center (Aalto-NMC). Prof. Pompea Del Vecchio is acknowledged for micro-DSC measurements on HFBII-FNP dispersions.

Open Access Funding provided by Politecnico di Milano within the CRUI-CARE Agreement.

Conflict of Interest

The authors declare no conflict of interest.

Data Availability Statement

Research data are not shared.

Keywords

^{19}F-MRI, coatings, fluorinated nanoparticles, fluorine, hydrophobin, protein corona, self-assembly

Received: September 2, 2021
Revised: October 31, 2021
Published online:

[1] a) J. Perrin, M. Capitao, M. Mougin-Degraef, F. Guérard, A. Faivre-Chauvet, L. Rbah-Vidal, J. Gaschet, Y. Guilloux, F. Kraeber-Bodéré, M. Chérel, J. Barbe, *Front. Med.* **2020**, *7*, 34; b) M. Saeed, Z. Xu, B. G. De Geest, H. Xu, H. Yu, *Bioconjugate Chem.* **2020**, *31*, 404; c) P. Gangadaran, R. L. Rajendran, B.-C. Ahn, *Cancers* **2020**, *12*, 1318; d) Y. Gao, C. Chu, A. Jablonska, J. W. M. Bulte, P. Walczak, M. Janowski, *WIREs Nanomed. Nanobiotechnol.* **2021**, *13*, e1688.

[2] a) E. J. Ngen, D. Artemov, *Int. J. Mol. Sci.* **2017**, *18*, 198; b) R. Yahyapour, B. Farhood, G. Graily, A. Rezaeyan, S. Rezapoor, H. Abdollahi, M. Cheki, P. Amini, H. Fallah, M. Najafi, E. Motevaseli, *Tissue Eng. Regener. Med.* **2018**, *15*, 249; c) N. J. Serkova, K. Glunde, C. R. Haney, M. Farhoud, A. De Lille, E. F. Redente, D. Simberg, D. C. Westerly, L. Griffin, R. P. Mason, *Cancer Res.* **2021**, *81*, 1189.

[3] H. E. Daldrup-Link, A. J. Theruvath, A. Rashidi, M. Iv, R. G. Majzner, S. L. Spunt, S. Goodman, M. Moseley, *Pediatr. Radiol.* **2021**, *27*, 1.

[4] a) I. Tirotta, V. Dichiarante, C. Pigliacelli, G. Cavallo, G. Terraneo, F. B. Bombelli, P. Metrangolo, G. Resnati, *Chem. Rev.* **2015**, *115*, 1106; b) H. Amiri, M. Srinivas, A. Veltien, M. J. van Uden, I. J. M. de Vries, A. Heerschap, *Eur. Radiol.* **2015**, *25*, 726; c) M. H. Cho, S. H. Shin, S. H. Park, D. K. Kadayakkara, D. Kim, Y. Choi, *Bioconjugate Chem.* **2019**, *30*, 2502; d) H. Lin, X. Tang, A. Li, J. Gao, *Adv. Mater.* **2021**, 2005657; e) P. Bouvain, S. Temme, U. Flögel, *WIREs Nanomed. Nanobiotechnol.* **2020**, *12*, e1639; f) M. Modo, *Neuroscience* **2021**, *474*, 37; g) X. Zhu, X. Tang, H. Lin, S. Shi, H. Xiong, Q. Zhou, A. Li, Q. Wang, X. Chen, J. Gao, *Chem.* **2020**, *6*, 1134.

[5] a) I. Tirotta, A. Mastropietro, C. Cordiglieri, L. Gazzera, F. Baggi, G. Baselli, M. G. Bruzzone, I. Zucca, G. Cavallo, G. Terraneo, F. B. Bombelli, P. Metrangolo, G. Resnati, *J. Am. Chem. Soc.* **2014**, *136*, 8524; b) K. Akazawa, F. Sugihara, T. Nakamura, H. Matsushita, H. Mukai, R. Akimoto, M. Minoshima, S. Mizukami, K. Kikuchi, *Angew. Chem., Int. Ed. Engl.* **2018**, *57*, 16742.

[6] a) C. Chirizzi, D. De Battista, I. Tirotta, P. Metrangolo, G. Comi, F. B. Bombelli, L. Chaabane, *Radiology* **2019**, *291*, 351; b) O. Koshkina, P. B. White, A. H. J. Staal, R. Schweins, E. Swider, I. Tirotta, P. Tinnemans, R. Fokkink, A. Veltien, N. K. van Riessen, E. R. H. van Eck, A. Heerschap, P. Metrangolo, F. B. Bombelli, M. Srinivas, *J. Colloid Interface Sci.* **2020**, *565*, 278; c) L. Jamgotchian, S. Vaillant, E. Selingue, A. Doerflinger, A. Belime, M. Vandamme, G. Pinna, W. L. Ling, E. Gravel, S. Mériaux, E. Doris, *Nanoscale* **2021**, *13*, 2373.

[7] a) S. E. Kirberger, S. D. Maltseva, J. C. Manulik, S. A. Einstein, B. P. Weegman, M. Garwood, W. C. K. Pomerantz, *Angew. Chem., Int. Ed.* **2017**, *56*, 6440; b) L. K. Hill, J. A. Frezzo, P. Katyal, D. M. Hoang, Z. B. Y. Gironda, C. Xu, X. Xie, E. Delgado-Fukushima, Y. Z. Wadghiri, J. K. Montclare, *ACS Nano* **2019**, *13*, 2969.

[8] M. B. Linder, G. R. Szilvay, T. Nakari-Setälä, M. E. Penttilä, *FEMS Microbiol. Rev.* **2005**, *29*, 877.

[9] a) B. W. Berger, N. D. Sallada, *J. Biol. Eng.* **2019**, *13*, 10; b) G. Dalkas, S. R. Euston, *Curr. Opin. Colloid Interface Sci.* **2019**, *41*, 1.

[10] a) D. Maiolo, C. Pigliacelli, P. Sánchez Moreno, M. B. Violatto, L. Talamini, I. Tirotta, R. Piccirillo, M. Zucchetti, L. Morosi, R. Frapolli, G. Candiani, P. Bigini, P. Metrangolo, F. B. Bombelli, *ACS Nano* **2017**, *11*, 9413; b) C. Pigliacelli, D. Maiolo, J. S. H. Nonappa, H. Amenitsch, C. Michelet, P. Sánchez Moreno, I. Tirotta, P. Metrangolo, F. B. Bombelli, *Angew. Chem., Int. Ed.* **2017**, *56*, 16186; c) C. Pigliacelli, A. D'Elicio, R. Milani, G. Terraneo, G. Resnati, F. B. Bombelli, P. Metrangolo, *J. Fluorine Chem.* **2015**, *177*, 62; d) S. Taniguchi, L. Sandiford, M. Cooper, E. V. Rosca, R. A. Khanbeigi, S. M. Fairclough, M. Thanou, L. A. Dailey, W. Wohlleben, B. von Vacano, R. T. M. de Rosales, P. J. Dobson, D. M. Owen, M. Green, *ACS Appl. Mater. Interfaces* **2016**, *8*, 4887.

[11] a) R. Milani, E. Monogioudi, M. Baldrighi, G. Cavallo, V. Arima, L. Marra, A. Zizzari, R. Rinaldi, M. Linder, G. Resnati, P. Metrangolo, *Soft Matter* **2013**, *9*, 6505; b) V. Dichiarante, R. Milani, P. Metrangolo, *Green Chem.* **2018**, *20*, 13; c) M. Dokouhaki, A. Hung, S. Kasapis, S. L. Gras, *Trends Food Sci. Technol.* **2021**, *111*, 378; d) L. Gazzera, R. Milani, L. Pirrie, M. Schmutz, C. Blanck, G. Resnati, P. Metrangolo, M. P. Krafft, *Angew. Chem., Int. Ed.* **2016**, *55*, 10263.

[12] a) L. Gazzera, C. Corti, L. Pirrie, A. Paananen, A. Monfredini, G. Cavallo, S. Bettini, G. Giancane, L. Valli, M. B. Linder, G. Resnati, R. Milani, P. Metrangolo, *Adv. Mater. Interfaces* **2015**, *2*, 1500170; b) G. R. Szilvay, K. Kisko, R. Serimaa, M. B. Linder, *FEBS Lett.* **2007**, *581*, 2721.

[13] a) M. Sarparanta, L. M. Bimbo, J. Rytkönen, E. Mäkilä, T. J. Laaksonen, P. Laaksonen, M. Nyman, J. Salonen, M. B. Linder, J. Hirvonen, H. A. Santos, A. J. Airaksinen, *Mol. Pharmaceutics* **2012**, *9*, 654; b) M. S. Grunér, U. Kauscher, M. B. Linder, M. P. Monopoli, *J. Proteomics* **2016**, *137*, 52. c) B. Niu, M. Li, J. Jia, C. Zhang, Y.-Y. Fan, W. Li, *J. Biomater. Sci., Polym. Ed.* **2020**, *31*, 1793.

[14] V. Dichiarante, M. I. Martinez Espinoza, L. Gazzera, M. Vuckovac, M. Latikka, G. Cavallo, G. Raffaini, R. Oropesa-Nuñez, C. Canale, S. Dante, S. Marras, R. Carzino, M. Prato, R. H. A. Ras, P. Metrangolo, *ACS Sustainable Chem. Eng.* **2018**, *6*, 9734.

[15] a) S. Y. Fam, C. F. Chee, C. Y. Yong, K. L. Ho, A. R. Mariatulqabtiah, W. S. Tan, *Nanomaterials* **2020**, *10*, 787; b) J. S. Suk, Q. Xu, N. Kim, J. Hanes, L. M. Ensign, *Adv. Drug Delivery Rev.* **2016**, *99*, 28; c) N. Giamblanco, G. Marletta, A. Graillot, N. Bia, C. Loubat, J.-F. Berret, *ACS Omega* **2017**, *2*, 1309; d) N. Ngadi, J. Abrahamson, C. Fee, K. Morison, *J. Appl. Sci.* **2010**, *10*, 3343.

[16] a) R. Mashiach, D. Cohen, L. Avram, T. Harris, I. Pinkas, L. Houben, H. Allouche-Arnon, A. Bar-Shir, *Nano Lett.* **2020**, *20*, 7207; b) R. Pujales-Paradela, T. Savic, D. Esteban-Gomez, G. Angelovski, F. Carniato, M. Botta, C. Platas-Iglesias, *Chem. - Eur. J.* **2019**, *25*, 4782.

[17] a) D. Walczyk, F. B. Bombelli, M. P. Monopoli, I. Lynch, K. A. Dawson, *J. Am. Chem. Soc.* **2010**, *132*, 5761; b) P. D. Pino, B. Pelaz, Q. Zhang, P. Maffre, G. U. Nienhaus, W. J. Parak, *Mater. Horiz.* **2014**, *1*, 301; c) L. Treuel, D. Docter, M. Maskos, R. H. Stauber, *Beilstein J. Nanotechnol.* **2015**, *6*, 857.

[18] D. Nierenberg, A. R. Khaled, O. Flores, *Rep. Pract. Oncol. Radiother.* **2018**, *23*, 300.

[19] F. Chapelin, C. M. Capitini, E. T. Ahrens, *J. Immunother. Cancer* **2018**, *6*, 105.
[20] a) M. P. Monopoli, D. Walczyk, A. Campbell, G. Elia, I. Lynch, F. B. Bombelli, K. A. Dawson, *J. Am. Chem. Soc.* **2011**, *133*, 2525; b) P. Jain, R. S. Pawar, R. S. Pandey, J. Madan, S. Pawar, P. K. Lakshmi, M. S. Sudheesh, *Biotechnol. Adv.* **2017**, *35*, 889.
[21] a) K. Partikel, R. Korte, D. Mulac, H.-U. Humpf, K. Langer, *Beilstein J. Nanotechnol.* **2019**, *10*, 1002; b) C.-Y. Lin, C.-M. Yang, M. Linden, *RSC Adv.* **2019**, *9*, 33912; c) D. Chen, S. Ganesh, W. Wang, M. Amiji, *Nanoscale* **2019**, *11*, 8760.
[22] a) S.-C. Zhao, L.-S. Ma, Z.-H. Chu, H. Xu, W.-Q. Wu, F. Liu, *Acta Pharmacol. Sin.* **2017**, *38*, 445; b) Y. Fujita, T. Yamashita, *Cell. Mol. Life Sci.* **2021**, *78*, 3907.
[23] V. Dichiarante, I. Tirotta, L. Catalano, G. Terraneo, G. Raffaini, M. R. Chierotti, R. Gobetto, F. B. Bombelli, P. Metarangolo, *Chem. Commun.* **2017**, *53*, 621.
[24] a) D. D. Silvio, N. Rigby, B. Bajka, A. Mayes, A. Mackie, F. B. Bombelli, *Nanoscale* **2015**, *7*, 11980; b) D. Doctor, U. Distler, W. Storck, J. Kuharev, D. Wunsch, A. Hahlbrock, S. K. Knauer, S. Tenzer, R. H. Stauber, *Nat. Protoc.* **2014**, *9*, 2030.
[25] a) E. Fasoli, P. G. Righetti, D. Moltrasio, A. D'Amato, *Anal. Chem.* **2015**, *87*, 1509; b) M. Nicoletti, C. Capodanno, C. Gambarotti, E. Fasoli, *Biochim. Biophys. Acta, Gen. Subj.* **2018**, *1862*, 2293.
[26] C. Chirizzi, C. Morasso, A. A. Caldarone, M. Tommasini, F. Corsi, L. Chaabane, R. Vanna, F. B. Bombelli, P. Metrangolo, *J. Am. Chem. Soc.* **2021**, *143*, 12253.